Carbohydrate Polymers 118 (2015) 60–69

Contents lists available at ScienceDirect

Carbohydrate Polymers

journal homepage: www.elsevier.com/locate/carbpol

Investigation of Salecan/poly(vinyl alcohol) hydrogels prepared by freeze/thaw method

Xiaoliang Qi, Xinyu Hu, Wei Wei, Hao Yu, Junjian Li, Jianfa Zhang, Wei Dong*

Center for Molecular Metabolism, Nanjing University of Science & Technology, 200 Xiaolingwei Street, Nanjing 210094, China

ARTICLE INFO

Article history:
Received 14 July 2014
Received in revised form 30 October 2014
Accepted 3 November 2014
Available online 20 November 2014

Keywords:
Salecan
Poly(vinyl alcohol)
Freeze–thaw processing
Hybrid hydrogels

ABSTRACT

Salecan is a novel water-soluble extracellular-glucan produced by a new kind of salt-tolerant strain *Agrobacterium* sp. ZX09 and can be applied in food and medicine industries. In this work, Salecan (Sal) was incorporated into poly(vinyl alcohol) (PVA) to prepare novel Sal/PVA hybrid hydrogels by repeated freeze–thaw processing. Physicochemical and biological characteristics of the hydrogels were investigated to evaluate their potential as cell adhesion materials. By increasing the Salecan content in the hybrid hydrogels, their swelling capacity increased notably, while the compressive modulus decreased. Observed by SEM, Sal/PVA hydrogels had a homogeneous porous structure. The degradation rate of the hydrogels can be controlled by tailoring the composition ratio of Sal/PVA. Furthermore, cells could adhere well on the surface of Sal/PVA hydrogels. In conclusion, these results make Sal/PVA hydrogels attractive materials for biomedical applications.

1. Introduction

Hydrogels are hydrophilic three-dimensional polymeric networks that can imbibe large quantities of water without dissolution or loss of their structural integrity. Because of their characteristic properties of high water content, together with their inherent mechanical strength, hydrogels have attracted considerable attention as promising materials for biomedical applications involved in drug carriers (El-Sherbiny, 2010), tissue engineering (El-Sherbiny & Yacoub, 2013), scaffolds for cell cultures (Almany & Seliktar, 2005), wound dressings (Yang et al., 2010) and filtration/separation processes (Dragan, 2014; El-Sherbiny, Abdel-Hamid, Rashad, Ali, & Azab, 2013). Both synthetic (Almany & Seliktar, 2005; Aouada, Pan, Orts, & Mattoso, 2009; Dinu, Přádný, Drăgan, & Michálek, 2013a,b) and natural polymers (Bortolin et al., 2012; Dragan & Apopei, 2013; Yang et al., 2010; Zhang & Edgar, 2014) can be used for the production of hydrogels, achieved by methods such as physical crosslinking, chemical gelation or self-assembly. In the last few years, hydrogels based on natural polymers, especially polysaccharides have been widely utilized due to its prominent biocompatibility, bioactivity, biodegradability, hydrophilicity and low toxicity (Aouada, Moura, Lopes da Silva, Muniz, & Mattoso, 2011).

Poly(vinyl alcohol) (PVA) is a water soluble synthetic polymer of great interest because of its many desirable characteristics (Yang et al., 2011). PVA hydrogels are non-toxic, noncarcinogenic, biocompatibility, good film forming ability and processability (Sahoo, Panyam, Prabha, & Labhasetwar, 2002). Applications of PVA hydrogels in the biomedical area include wound dressing (Kim et al., 2008), artificial articular cartilages (Kobayashi & Oka, 2004) and drug delivery (Ossipov, Kootala, Yi, Yang, & Hilborn, 2013). PVA gels can be prepared via chemical or physical crosslinking. Although the chemical crosslinking methods could efficiently prevent the dissolution and enhance the mechanical properties of PVA hydrogels, the potential toxic environments, which are created from chemical crosslinking, may have harmful effects on cells. Thus, researchers are attempting to stay away from this method (Slaughter, Khurshid, Fisher, Khademhosseini, & Peppas, 2009).

In contrast, PVA physical hydrogels (prepared by freeze–thawing process) have drawn a greater research attention. Cryotropic treatment (single or repeated cycles of freeze–thawing) of concentrated PVA aqueous solution induces crystallization and leads to the formation of a network structure in which PVA crystallites acted as junction points (Hassan & Peppas, 2000a,b). This method addresses toxicity issues because it does not result in the reagent residuals and chemical toxicity, and consequently, no toxicity agents are leaching out from the gel matrix (Kim et al., 2008). Furthermore, these physically cross-linked hydrogels, which are inter-connected by hydrogen bonding, exhibit more porous, spongy, rubbery and higher elastic properties than PVA hydrogels prepared by other methods (Hassan & Peppas, 2000a; Plieva

* Corresponding author. Tel.: +86 25 84318533; fax: +86 25 84318533.
E-mail address: dongwei@njust.edu.cn (W. Dong).

http://dx.doi.org/10.1016/j.carbpol.2014.11.021
0144-8617/

et al., 2006). Nowadays these gel matrices have been widely implemented in biotechnology fields, specifically in molecules (protein, peptides) (Hassan & Peppas, 2000a) and whole cell immobilization (Lozinsky & Plieva, 1998). However, pertinent to certain biomedical applications, being conducive to cell adhesion is an essential requirement. Regretfully, PVA cryogels are intrinsically bio-inert like most synthetic hydrogels and non-adhesive to cells and proteins. An effective way to overcome this drawback is to integrate PVA hydrogel with natural polymers (such as proteins and polysaccharides) to form blending hydrogels (Liu, Vrana, Cahill, & McGuinness, 2009).

Salecan is a new extracellular water-soluble microbial polysaccharide (Cas. No. 1439905-58-4) produced by strain of *Agrobacterium* sp. ZX09. This novel strain was isolated from soil samples collected from ocean coast of Shandong province, PR China by our laboratory in 2009 and its 16S rDNA sequence was deposited in the GenBank database with accession No. GU*810841 (Xiu et al., 2010). Large scale production of Salecan is low cost, convenient and easy processing. Salecan is a linear (1 → 3)-β-D-glucan comprising β-1-3-linked glucopyranosyls with a small number of α-1-3-linked, and is composed of the following repeating unit: → 3)-β-D-Glcp-(1 → 3-[β-D-Glcp-(1 → 3)-β-D-Glcp-(1 → 3)]3-α-D-Glcp-(1 → 3)-α-D-Glcp-(1 → (see Fig. S1 in Supporting information) (Xiu et al., 2010). This unique linkage pattern, was reported by our laboratory in 2010, endows Salecan with prominent biological activities including anti-oxidation and non-toxicity (edible safety) (Chen et al., 2011; Xiu et al., 2011a; Xiu, Zhou, Zhu, Wang, & Zhang, 2011b). Salecan can be utilized in food fields as a new source of thickening additive (Chen et al., 2012; Xiu et al., 2011a,b) and medical fields for preventing and treating constipation *CN Pat.*, 102058616A, 2011. Furthermore, Salecan also has distinctive physicochemical properties: (i) Salecan ($M_w = 2 \times 10^6$ Da) solutions are highly viscous even at low polymer concentrations (Xiu et al., 2011a,b); (ii) Salecan possesses a large amount of pendant hydroxyl functional groups making it prone to chemical modification (Meng, Matson, & Edgar, 2014). These features make it an excellent candidate for the preparation of hydrogel. In the past, our group has already studied the properties of Salecan-based hydrogels (Hu et al., 2014a,b). Hu et al. (2014b) found that cells could not grow on the surface of the pure PAAm (polyacrylamide) hydrogel, but it could adhere well on the surface of the Salecan/PAAm semi-IPN hydrogels due to the addition of Salecan (Hu et al., 2014b). These results remind us that the incorporation of Salecan into the PVA cryogels may enhance the cell adhesion.

In this work, we report the synthesis of Sal/PVA blended cryogels by the freeze-thaw technique. The novelty of the present study is to evaluate the cell adhesion ability of bio-inert PVA cryogels with the use of Salecan for the first time. Furthermore, their physicochemical properties, such as gel fraction, swelling behavior, thermal stability, morphology and mechanical strength were also investigated. Due to its biomimetic composition and a green fabrication procedure, the novel Sal/PVA hybrid hydrogels have great potential in biomedical engineering.

2. Experimental

2.1. Materials

PVA (average $M_w = 125{,}000$ g/mol, degree of polymerization ~2800, degree of hydrolysis 98.0–98.8 mol%) was obtained from Sigma–Aldrich Chemie GmbH, Riedstr., Germany. Salecan (average $M_w = 2000{,}000$ g/mol, Xiu et al., 2010) was made by Center for Molecular Metabolism, Nanjing University of Science & Technology. 3-(4,5-dimethylthiazol-2-yl)-2-5-diphenyltetrazolium bromide (MTT), dimethyl sulfoxide and penicillin/streptomycin, all purchased from Nanjing KeyGen Biotech Co., Ltd (China), were used as received.

Table 1
The preparation and the compositions of Sal/PVA solutions.

Ingredient	Designation					
	Pure PVA	S10V90	S20V80	S30V70	S40V60	S50V50
Salecan (2%,w/v) (mL)	0	10	20	30	40	50
PVA (10%,w/v) (mL)	100	90	80	70	60	50

2.2. Fabrication of Sal/PVA hybrid hydrogels

Sal/PVA hydrogels were obtained by freezing–thawing (F–T) cycle (Peppas & Stauffer, 1991). The preparation scheme is presented in Fig. 1. First, 10.0 g PVA was added to 100 mL deionized water and stirred continuously at 90 °C for 2 h to form a homogeneous solution of 10% (w/v). Salecan solution (2%, w/v) was prepared by dispersing the required amount of Salecan in deionized water under moderate stirring at 60 °C for 2 h. The PVA and Salecan solutions were cooled to room temperature prior to assessment. Then, a volume of Salecan solution was mixed with the PVA solution at five ratios, as listed in Table 1. When the volume of Salecan solution was higher than 50% (v/v), the mixture was too diluted that cannot form a hydrogel. The blends stirred vigorously with mechanical stirrer at room temperature for 2 h. The homogeneous Sal/PVA solution was sonicated in an ultrasonic bath at room temperature for 0.5 h to get rid of air bubbles. Finally, the mixtures were poured in petri dishes, followed by freezing at −20 °C for 18 h and thawing at 25 °C for 6 h, for three consecutive cycles. All samples were left in de-ionized water for 72 h to extract leachable sol fraction from polymer matrix for further characterizations and the influence of Salecan concentration on the gel fraction is shown in Fig. S2 (Supporting information).

2.3. Fourier transform infrared (FTIR) spectroscopy

FTIR spectra of the cryogels were recorded on an FTIR spectrometer (Nicolet IS-10) working in attenuated total reflectance mode, within a spectral range of 400–4000 cm^{-1}.

2.4. X-ray diffraction measurements (XRD)

Wide-angle XRD patterns of the dried hydrogels were measured using an X-ray generator (PW 1720, Philips) operated at a voltage of 30 kV and current of 20 mA with Cu$K\alpha$ radiation ($\lambda = 0.154$ nm) in the 2θ range of 5–60°. The relative degree of crystallinity was calculated according to the method described in the literature (Costa-Júnior, Barbosa-Stancioli, Mansur, Vasconcelos, & Mansur, 2009).

2.5. Differential scanning calorimetry (DSC)

DSC experiments were performed with a differential scanning calorimetry (DSC, Mettler Toledo 823/e) under nitrogen purge gas and at a heating rate of 10 °C/min in the temperature range of 25–300 °C. The T_g was taken at the midpoint of the baseline shift (Fathi, Atyabi, Imani, & Alinejad, 2011). The degree of crystallinity (%) was calculated as:

$$\text{degree of crystallinity}\,(\%) = \left(\frac{\Delta H}{\Delta H_0}\right) \times 100$$

where ΔH was determined by integrating the area under the melting peak of the PVA based hydrogel over the range 200–250 °C, ΔH_0 was the thermodynamic enthalpy required to melting a 100% crystalline PVA (138.6 J/g) (Peppas & Hansen, 1982).

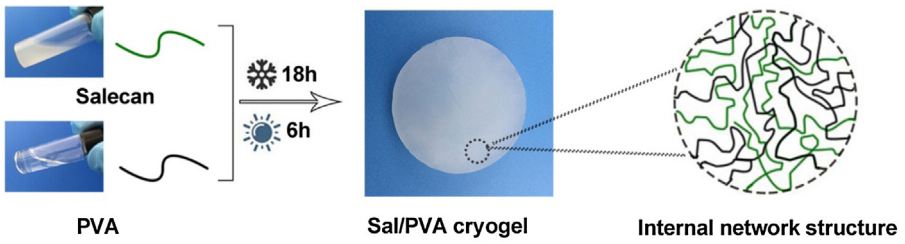

Fig. 1. Schematic representation of the formation of Sal/PVA blending hydrogels.

2.6. Thermo gravimetric analysis (TGA)

The thermal behavior of the samples was performed with a TA Model Q600 thermal gravimetric analyzer under a nitrogen atmosphere and at a heating rate of 10 °C/min in the temperature range of 25–600 °C.

2.7. Swelling behavior

The dried hydrogels were immersed in an excess of deionized water at room temperature. The swollen samples were weighed at definite time intervals after wiping off the excessive surface water with wet filter paper. The swelling ratio (SR) of the hydrogel was determined using the following equations:

$$SR = \frac{(W_t - W_d)}{W_d}$$

where W_t was the weight of the swollen hydrogel at time t and W_d was initial weight of the hydrogel. The swelling kinetics in 0.9 wt% NaCl solution was tested in the same way. The equilibrium water content (EWC) was calculated as follows:

$$\mathrm{EWC}(\%) = \left[\frac{(W_e - W_0)}{W_e}\right] \times 100$$

where W_e was weight of the swollen hydrogel at equilibrium.

2.8. Water retention studies

Prior to the water retention studies, the hydrogel samples were allowed to swell till equilibrium in distilled water at room temperature, and then the equilibrium swollen hydrogels were quickly transferred into an oven at a temperature of 37 °C to record the weight during collapsing at predetermined time intervals. Water retention (WR) of the hydrogels was defined as follows:

$$\mathrm{WR}(\%) = \left(\frac{W_t}{W_{eq}}\right) \times 100$$

where W_t was the weight of hydrogel at different intervals during the shrinking process and W_{eq} was the weight of the swollen hydrogel at equilibrium.

2.9. Microstructural morphology

The surface morphology of the hydrogels after being freeze dried was investigated by scanning electron microscope (JSM-6360LV, JEOL, Japan) using 30 kV voltage. Prior to observation, the freeze dried fracture sections were coated with a thin layer of gold to enhance conductivity.

2.10. Rheological characterization

The rheological measurements were conducted on an Anton Paar MCR101 rheometer, using a parallel plate geometry with a diameter of 50 mm and a gap value of 1 mm. Dynamic viscoelastic measurements were carried out at a small strain (0.01%) which ensured that the deformation imposed on the hydrogels were performed in the linear viscoelastic region. Viscoelastic properties were measured in 0.1–10 Hz frequency range. The storage modulus (G') and loss modulus (G'') of the cryogels were plotted as a function of frequency.

2.11. Mechanical properties test

The Compressive mechanical properties of the cylindrical Sal/PVA hydrogels were tested using an Instron 4464 mechanical tester equipped with a 500 N load cell at room temperature. The hydrogel samples (column, diameter 20 mm and height 10 mm) were compressed at a rate of 2 mm/min. The compressive modulus was obtained by the initial (straight line) linear slope of the stress versus strain curve.

2.12. In vitro degradation

Degradation of the samples (2 × 1 cm and known weight) was evaluated by incubating hydrogels in a pH 7.4 phosphate buffered saline solution (PBS) containing 0.02 wt% sodium azide at 37 °C. The PBS solution was changed weekly. At pre-selected time points, the remaining hydrogels were removed from the buffer solution and dried in a vacuum drier at 60 °C to constant weight. The percent weight remaining (WR) of each sample was determined by using the following equation:

$$\mathrm{WR}(\%) = \frac{W_t}{W_0} \times 100$$

where W_0 and W_t were the sample weights before and after the degradation, respectively.

2.13. Cell experiment

2.13.1. Cell culture

The COS-7 fibroblast cell line was used in the assay. Cells were incubated in Dulbecco's modified eagle medium (DMEM) containing 10 vol% fetal bovine serum (FBS), 200 mM L-glutamine, 2 mg/mL sodium bicarbonate and 100 μg/mL penicillin/streptomycin. Cells were cultured at 37 °C in a humidified air incubator, and the medium was changed every 3 days.

2.13.2. Cell viability assay

The cytotoxicity of hydrogels was tested based on the guideline of international standard ISO 10993-5. Freeze-dried samples were sterilized by immersing in 70% (v/v) ethanol for 1 h, followed by washing extensively with sterile PBS (pH 7.4) for five times to remove alcohol components. The sterile hydrogels were then incubated with 5 mL of DMEM (containing 10% bovine serum albumin, 1% penicillin/streptomycin) at 37 °C. After incubation for 4 and 7 days, all hydrogels were gently removed and the extracts retained and evaluated for cytotoxicity. Cytotoxicity of the hydrogels to

COS-7 cells was examined by a 3-(4,5-dimethylthiazol-2-yl)-2,5-diphenyltetrazolium bromide (MTT) cell viability assay. In addition, fresh DMEM medium (without the extract of hydrogels) was used as a negative control.

2.13.3. Cell seeding

Gels were sterilized by immersing in 70% (v/v) ethanol for 1 h, and then washed by sterilized PBS (pH 7.4) and cell-free culturing medium three times, respectively. Prior to seeding cells, the sterile samples were transferred to 24-well plates. After that, COS-7 cells were then seeded on the surface of the hydrogels at an initial density of 1×10^4 cells/well and were incubated at 37 °C in a 5% CO_2 incubator. The medium was changed every 2 days.

2.13.4. Cell observations

After 5 days of culture on the pure PVA hydrogel and Sal/PVA hydrogels, cells were rinsed gently with PBS (37 °C, pH 7.4) to remove non-adherent cells. Each sample was then fixed with 4% paraformaldehyde in PBS for 30 min and subsequently permeabilized with 0.1% (v/v) Triton X-100 for 10 min. After that, all the samples were washed thoroughly with PBS three times, prior to observation under a fluorescence microscope (Olympus, Japan).

2.14. Statistical analysis

All data were presented as means ± standard deviations. Comparisons among the three groups were made with one-way analysis of variance.

3. Results and discussion

3.1. FTIR analysis

The consecutive F–T cycles led to the formation of entangled Sal/PVA hydrogels. These hydrogels were a matrix of physically cross-linked polymeric chains, non-cross-linked polymers and water (Sung et al., 2010). In order to clarify the formation mechanism for Sal/PVA blending hydrogels, FTIR spectra of Salecan, pure PVA and Sal/PVA hydrogels were quantitatively studied, as presented in Fig. 2(a). The FTIR spectra of Salecan showed a broad band appeared at 3291 cm^{-1}, indicating stretching of hydroxyl groups. Peaks at the 1100–800 cm^{-1} region were assigned to polysaccharide structure. Specifically, the peak at 1040 cm^{-1} represented C—OH stretching in glucopyranose ring, peak at 893 cm^{-1} confirmed that D-glucopyranose had a β-configuration and peak at 814 cm^{-1} was attributed to the presence of a little α-glucopyranose (Xiu et al., 2010). In case of pure PVA hydrogel, a broad peak at 3300 cm^{-1} was due to the O—H stretching vibration of hydroxyl group of PVA. The peak at 2940 cm^{-1} was associated with the stretching vibration of —CH_2. The sharp peak at 1735 cm^{-1} assigned to the C=O stretching of the acetate group of PVA (Costa-Júnior et al., 2009; Mansur,Costa, Mansur, & Barbosa-Stancioli, 2009). The peak observed at 1335 cm^{-1} has been ascribed to combination frequencies of (CH—OH). A characteristic peak verified at 1141 cm^{-1} was related to the C—O stretching vibration, which was mostly attributed to the crystallinity of the PVA (Hassan & Peppas, 2000a). Compared to the IR spectrum of pure PVA, there was no significant different between the peaks of pure PVA and the Sal/PVA hydrogel (S50P50). Salecan did not influence essentially the intensities of the groups from PVA. However, it can be clearly observed that bands corresponding to O—H stretching vibration showed a blue shift, from 3280 cm^{-1} (pure PVA) to 3312 cm^{-1} (S50P50), meaning disruption of hydrogen bonds between the polymer chains (Fathi et al., 2011). In addition, the intensity of peak at 1140 cm^{-1} (C—O stretching) corresponding to crystallinity of the PVA was significantly decreased as the Salecan concentration increased (Huang et al., 2012). Thus, from the FTIR results, it suggested the presence of Salecan and PVA in the prepared cryogels.

Table 2
DSC data of hydrogel samples.

	T_g (°C)	T_m (°C)	ΔH_M (J/g)	Crystallinity (%)
Pure PVA	62.5	224.9	73.1	52.8
S10P90	63.8	224.1	60.5	43.6
S20P80	65.0	223.9	57.2	41.3
S30P70	67.8	223.5	55.5	40.0
S40P60	70.1	222.9	51.4	37.1
S50P50	71.5	222.0	48.2	34.8

3.2. X-ray diffraction studies

X-ray diffraction patterns of the hydrogels are depicted in Fig. 2(b). The amorphous nature of the Salecan can be proven by XRD characterization, since no sharp peaks can be seen in the XRD pattern, only had a very broad hole around 20° (Hu et al., 2014a). Dried pure PVA hydrogel exhibited a characteristic diffraction peak (strong) at $2\theta = 19.4°$, corresponding to its (1 0 1) crystal planes (Bai, Li, Wang, & Shi, 2010; Nishio & Manley, 1988). The XRD patterns of Sal/PVA composites were different from those of pure PVA and Salecan. With the increase of proportion of Salecan, the diffraction peak corresponding to $2\theta = 19.4°$ of PVA became gradually lowered and the relative degree of crystallinity (%) of S10P90, S20P80, S30P70, S40P60 and S50P50 were 60.0, 48.1, 41.2, 32.5 and 21.9, respectively, thus indicating the change of PVA from its crystalline to amorphous state. The amorphous region of PVA polymer matrix augmented due to addition of Salecan. This result was mainly due to the strong intermolecular hydrogen bonding interaction occurred between these two components (Cascone, Maltinti, Barbani, & Laus, 1999).

3.3. DSC analysis

The DSC curves of Salecan, pure PVA and Sal/PVA hydrogels are shown in Fig. 2(c) and the full set of thermal data in Table 2. As can be seen from Fig. 2(c), the glass transition temperature (T_g) of the Salecan could be at around 116 °C and the T_g of pure PVA gel was measured to be 62.5 °C, which was very close to the reported value (about 68 °C) (Cascone et al., 1999). The T_g value of Sal/PVA blends was between the Salecan and pure PVA, and it increased linearly with increasing Salecan content from 63.8 °C (S10P90) to about 71.5 °C (S50P50), suggesting the miscibility of Salecan with PVA. The notable increase in T_g values was mainly due to higher T_g of Salecan and its good miscibility with PVA matrix. Meanwhile, the Sal/PVA blends exhibited a single T_g that was shifted to higher temperature with increasing amount of Salecan, indicating strong interactions between PVA and Salecan (Fathi et al., 2011).

In addition, according to the Salecan curve, there was an endothermic peak at 283 °C, which could be attributed to the dissociation process of interchain hydrogen bonding of Salecan. Furthermore, with the increase of the Salecan content, the sharp endothermic peak of hydrogels turned into broader and their melting points (T_m) were slightly decreased, from 225.0 °C (pure PVA) to 220.0 °C (S50P50). Since there was no chemical modification between Salecan and PVA, it can be considered that the decrease of melting temperature was possibly due to conformational changes within the polymer chains. The conformational changes involve the size of the crystallites and the degree of crystallinity (Hassan & Peppas, 2000b). The degree of crystallinity (%) of the gels were 52.8 (pure PVA), 43.6 (S10P90), 41.3 (S20P80), 40.0 (S30P70), 37.1 (S40P60) and 34.8 (S50P50), respectively. The depressions in melting point and percent crystallinity indicated that the incorporation of Salecan weakened the interaction between PVA chains and

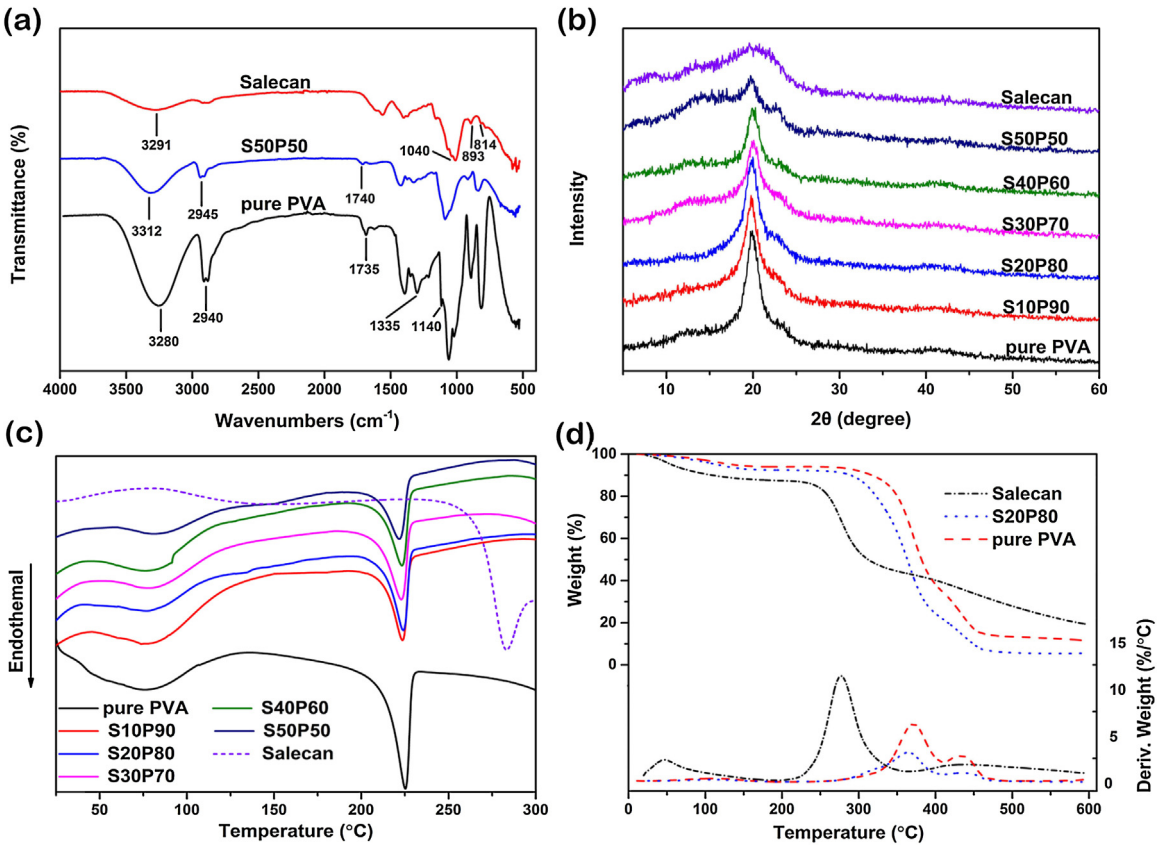

Fig. 2. FTIR (a), XRD (b), DSC (c) and TGA (d) curves of Salecan, pure PVA and Sal/PVA hydrogels.

hindered the crystallization of PVA. The trend excellently corroborated net crystallinity data calculated from X-ray diffraction analysis.

3.4. TGA measurements

TGA and DTG diagrams of Salecan, pure PVA and S50P50 are shown in Fig. 2(d). Salecan started decomposing after 150 °C and mass loss (11.77%) up to 180 °C can be ascribed to the loss of free and bound water. Subsequently, mass loss (43.78%) occurred at 180 °C to 350 °C, further a 23.67% of mass loss was observed between 350 °C and 575 °C and reached a value of 80.60% at 600 °C. This may be attributed to the cleavage of functional groups, followed by decomposition of the main skeleton of Salecan (Hu et al., 2014a). Both neat PVA and their composites exhibited a two-step degradation: a small mass loss (5.99%) starting below 150 °C, presumably due to the elimination of the residual water trapped in the PVA matrix; and a large loss (about 70%) took place in the temperature range of 230–550 °C, presumably due to degradation of Salecan, de-polymerization of PVA chain and decomposition of hydrogel networks. Comparing with S20P80, the curve of the pure PVA was shifted toward a slightly higher temperature. From the TG curves, it can be concluded that the presence of Salecan in the network negatively affected thermal stability of PVA hydrogels. Furthermore, it can be observed from the DTG curves that T_d (the degradation temperature corresponding to the maximum mass loss rate) was present at 277 °C for Salecan, 348 °C for S20P80 and 371 °C for pure PVA, respectively. This also indicated that the thermal stability of Salecan was improved upon by forming Sal/PVA composite hydrogels, because the hydroxyl groups of PVA formed hydrogen bond crosslinking with hydroxyl groups of Salecan, which limited the chain movement during thermal treatment (Lin, Yu, & Yang, 2006).

3.5. Swelling behavior

The swelling of the hydrogels in deionized water over time is presented in Fig. 3(a). As can be seen, the swelling ability of the Sal/PVA hydrogels increased with raising the Salecan content. S50P50 showed a maximum swelling ratio of 13.7, compared to 5.1 in case of the pure PVA. Generally speaking, lesser cross-linked hydrogels tended to show higher water uptake ability, because the highly cross-linked structure could not sustain much water within gel structure (Balakrishnan, Mohanty, Umashankar, & Jayakrishnan, 2005). For the Sal/PVA hydrogels, when the PVA content decreased, the physical cross-linked density of the hydrogels network decreased and molecular entanglement between Salecan and PVA was weakened, which led to the improvement of the hydrogel swelling ability. In the same time, the swelling capability was strongly influenced by the overall hydrophilicity of the resulting hydrogel (Kaity, Isaac, & Ghosh, 2013). By enhancing the amount of Salecan, the hydrogel networks became more hydrophilic and consequently absorbed more water, resulting in an improvement of swelling.

Fig. 3(b) shows the swelling ratio values of the hydrogels in deionized water and in 0.9 wt% NaCl solution. It can be concluded that the swelling ratios of the cryogels in 0.9 wt% NaCl solution were much lower than in deionized water. This was because that the increment of ionic strength decreased the osmotic pressure difference between gel network and external solution, which hindered the water molecules to penetrate into the network.

Fig. 3(c) displays the equilibrium water content (EWC) of the obtained hydrogels. With the increase of the Salecan content, EWC values were observed to change slightly from about 84% to 92% in deionized water and 70% to 80% in 0.9 wt% NaCl solution, respectively. These results further confirmed that the ionic strength of a

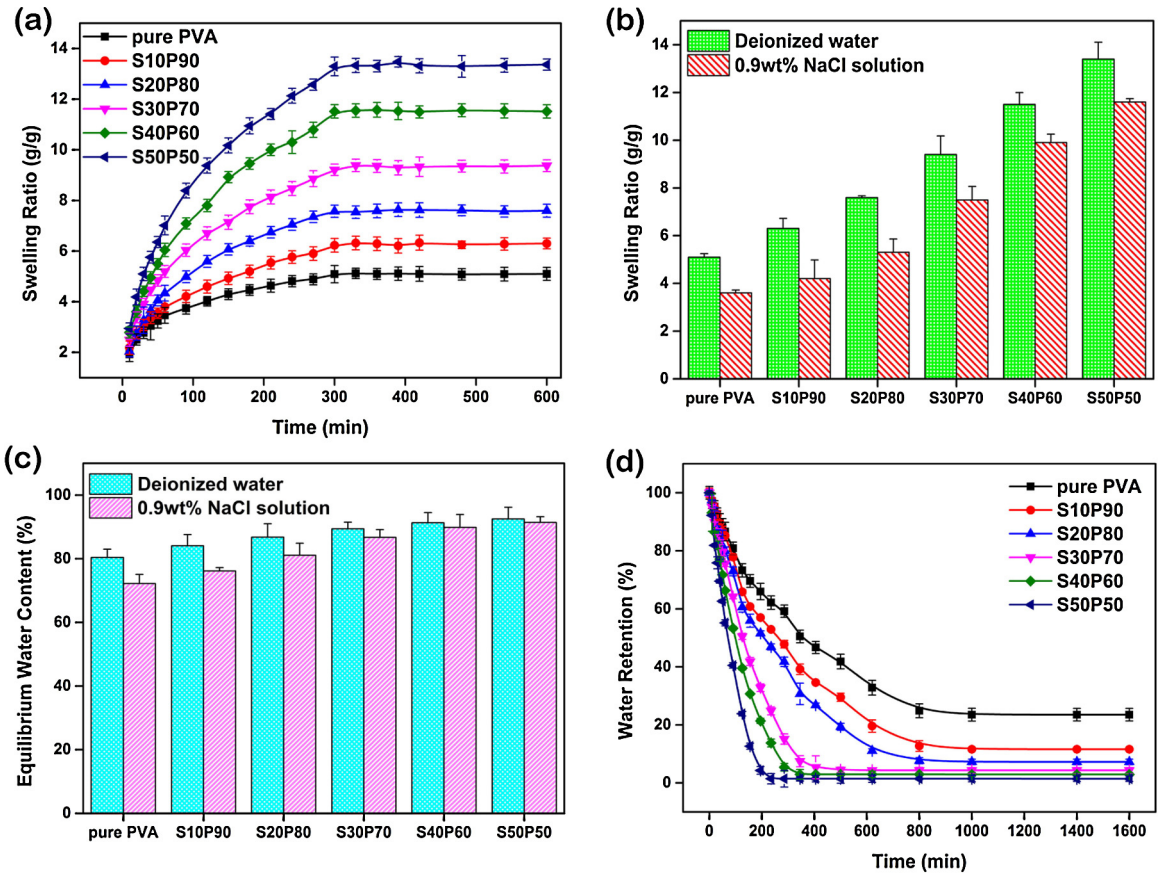

Fig. 3. Swelling ratio values in deionized water (a), Swelling kinetics in deionized water and in 0.9 wt% NaCl solution (b), equilibrium water content (c) and water retention graphs (d) of pure PVA and Sal/PVA hydrogels.

medium had a vital influence on the swelling capabilities of hydrogels.

3.6. Water retention test

The water retention ability of the hydrogels is illustrated in Fig. 3(d). It can be clearly seen that a cryogel containing greater PVA and lesser Salecan showed greater water retention capacity. In addition, the rate of water loss decreased with increasing PVA content. For instance, within 1000 min, pure PVA, S10P90, S20P80, S30P70, S40P60, S50P50 shrank and lost about 76.5%, 88.4%, 92.8%, 95.7%, 97.1% and 98.6% water, respectively. These results can be explained by the fact that the presence of more PVA in the gels enhanced the physically crosslinking density of the network, which in turn restricted mobility and relaxation of the polymeric chains and, therefore, the hydrogel became harder to lose water.

3.7. SEM results

Fig. 4 depicts the SEM image of cross-section morphologies of the cryogels. According to Fig. 4, the pure PVA hydrogel (Fig. 4(a)) presented a smooth, continuous and no pore shape structure, which may be attributed to the crystallization of PVA (Wu, Gong, Fan, & Xia, 2011). However, the Sal/PVA samples (Fig. 4(b)–(f)) exhibited an interconnected porous structure with regular pore distribution. The average pore size declined with increasing PVA content. For example, S50P50 had the largest pore size of approximately 13.2 μm, while the pore size shifted to about 8.6 μm, 7.3 μm, 4.9 μm and 2.8 μm in the case of S40P60, S30P70, S20P80 and S10P90, respectively. This morphological trend gave a better explanation to the swelling capacity and water evaporation behaviors of the gels (see Sections 3.5 and 3.6). As the Sal/PVA volume ratio increased, the physical crosslinking density of the hydrogel decreased, leading to the water content of hydrogel increased. In the freeze-dried process (hydrogels dehydrated by lyophilization), the free water was frozen into larger ice crystals which were eventually represented by larger pores (Dinu et al., 2013a,b). These results indicated that the composition ratio of Sal/PVA played a significant role in the tuning of the size and shape of the pore in the obtained freezing–thawing hydrogels. Furthermore, a porous surface with different pore size distribution, which can facilitate permeation of nutrients in and cellular products out of the gel, was beneficial for cell growth (Autissier, Le Visage, Pouzet, Chaubet, & Letourneur, 2010).

3.8. Rheological analysis

Fig. 5(a) and (b) presents the linear viscoelastic frequency sweep response of the pure PVA and Sal/PVA hydrogels. As can be observed, all hydrogels showed typical gel rheological behavior. The storage modulus (G') of the hydrogel was larger than the loss modulus (G'') over the entire tested angular frequencies in the range between 0.1 and 10 Hz, indicating that the hydrogels were highly elastic (Hernández, Sarafian, López, & Mijangos, 2004). For all the prepared hydrogels, both the G' and G'' values increased with the increasing of the PVA concentration, from S50P50 to pure PVA. This suggested that the freezing–thawing gelation enhanced the density of polymer network and decreased the flexibility of chains via the development of hydrogen bonding by introduction of more PVA chains (Holloway, Spiller, Lowman, & Palmese, 2011). It also demonstrated that the PVA molecular chains played a

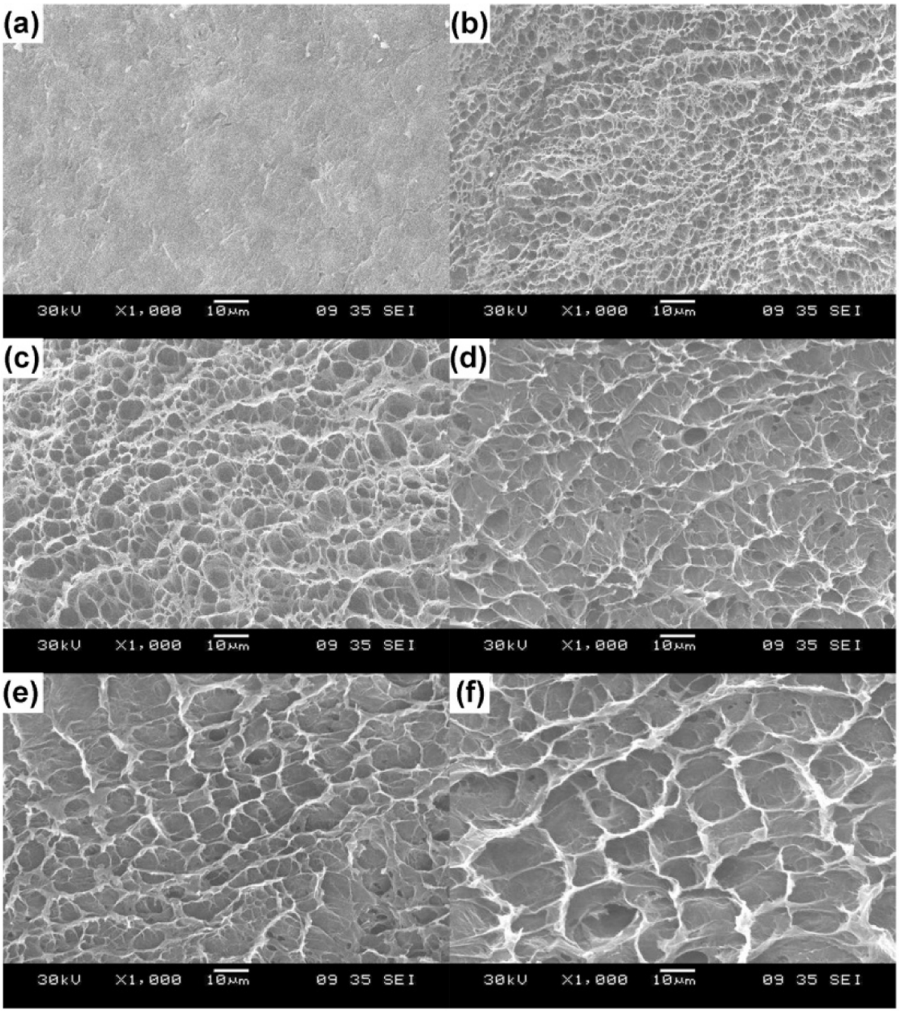

Fig. 4. SEM photos of pure PVA and Sal/PVA hydrogels: (a) pure PVA, (b) S10P90, (c) S20P80, (d) S30P70, (e) S40P60, (f) S50P50. Scale bars represent 10 μm.

predominant role on the improving of mechanical strength of the composite hydrogels.

3.9. Mechanical properties

To investigate the influence of Salecan on the mechanical properties of the hydrogels, their stress–strain curves are displayed in Fig. 5(c) and the results of fracture strain, compressive strength and compressive modulus are summarized in Table S1 (Supporting information). Both compressive strength and modulus showed a decreasing trend with an increase in polysaccharide amount. Specifically, the pure PVA hydrogel yielded the highest compressive strength and modulus, while these values of the hybrid hydrogels decreased as the proportion of Sal/PVA increased. For example, the compressive modulus of the hydrogels decreased considerably with the increase of Salecan content from 145 kPa (pure PVA) to 23 kPa (S50P50). These results demonstrated that the blending of Salecan caused the sample less stiff. In addition, Fig. 5(c) shows that with the increase of Salecan, the compressive strength reduced gradually from 164 kPa (pure PVA) to 134 kPa (S50P50) while the fracture strain increased from 71% (pure PVA) to 84% (S50P50). This phenomenon suggested that the incorporation of Salecan made the sample to become more ductile (Sung et al., 2010).

In order to explain this, it should be considered that when Salecan was blended with PVA, the cross-linking density of the hydrogel was the major factor which affected the compressive mechanical properties of the Sal/PVA hydrogels. This can be attributed to the hydrogen bonding or intermolecular interactions between the chains of PVA and Salecan. Our results indicated that the crosslink between PVA and Salecan was not strong compared to the crosslink between PVA itself. In other words, the orderliness of the molecular arrangement was interfered by Salecan. Thus, whereas PVA was hard and close to solid, the resulting Sal/PVA hydrogels exhibited more flexibility and elasticity. Similar results were observed for other polysaccharide/PVA blending hydrogels (Huang & Yang, 2008; Sung et al., 2010).

3.10. In vitro degradation

The controlled degradation of hydrogels plays a crucial role in regulating cell proliferation and tissue regeneration. Ideally, hydrogels as tissue engineering scaffolds should be degradable at a rate proportional to formation of new tissue (Gnanaprakasam Thankam, Muthu, Sankar, & Kozhiparambil Gopal, 2013; Hassan, Ward, & Peppas, 2000). The degradation profiles of the Sal/PVA cryogels after 60 days (expressed as a % weight remaining) are illustrated in Fig. 6(a). As apparent from the figure, degree of degradation of pure PVA cryogel was found to be 35% while S50P50 cryogel reached to 77% within 60 days. For S10P90, S20P80, S30P70 and S40P60, the degree of degradation was 40%, 47%, 52% and 60%, respectively. This phenomenon demonstrated that the stability of blend hydrogels was dramatically increased with decreasing the ratio of Sal/PVA.

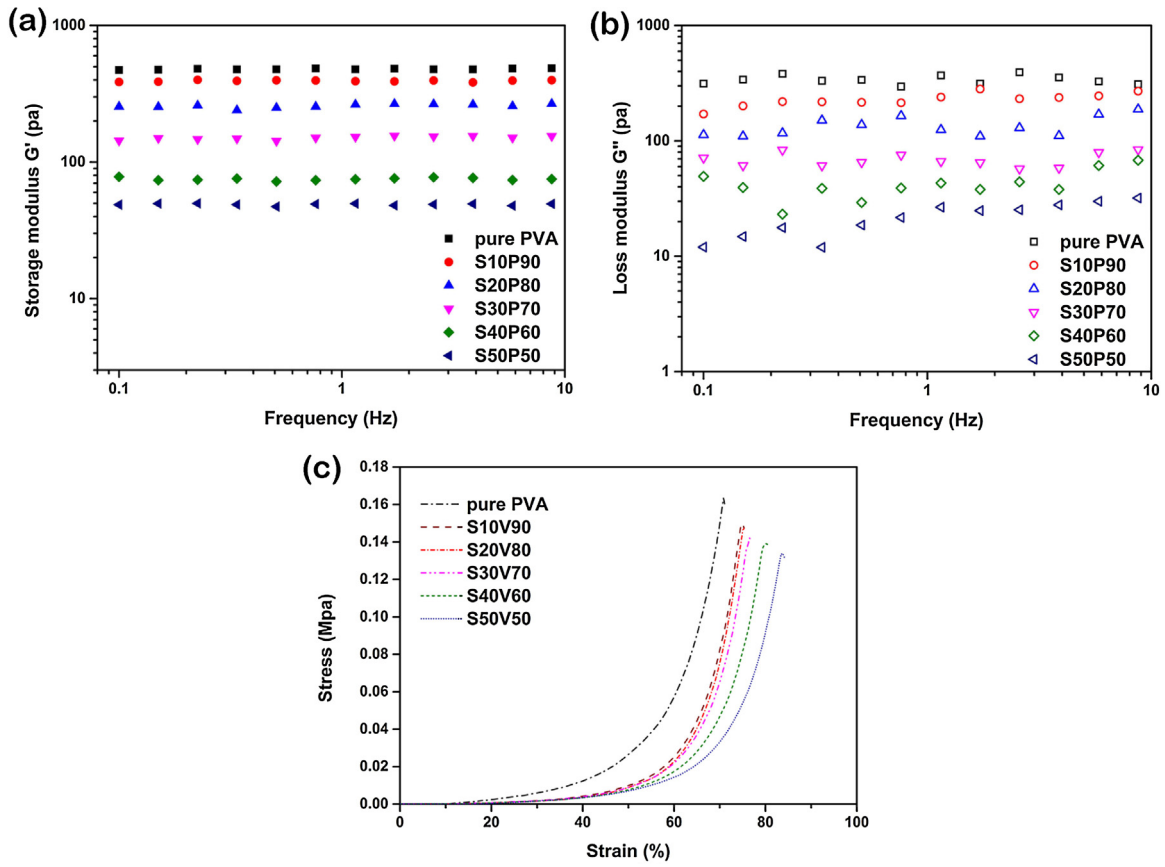

Fig. 5. Frequency dependence of (a) dynamic storage modulus (G') and (b) dynamic loss modulus (G'') of pure PVA and Sal/PVA hydrogels. (c) Representative stress–strain curves of pure PVA and Sal/PVA hydrogels.

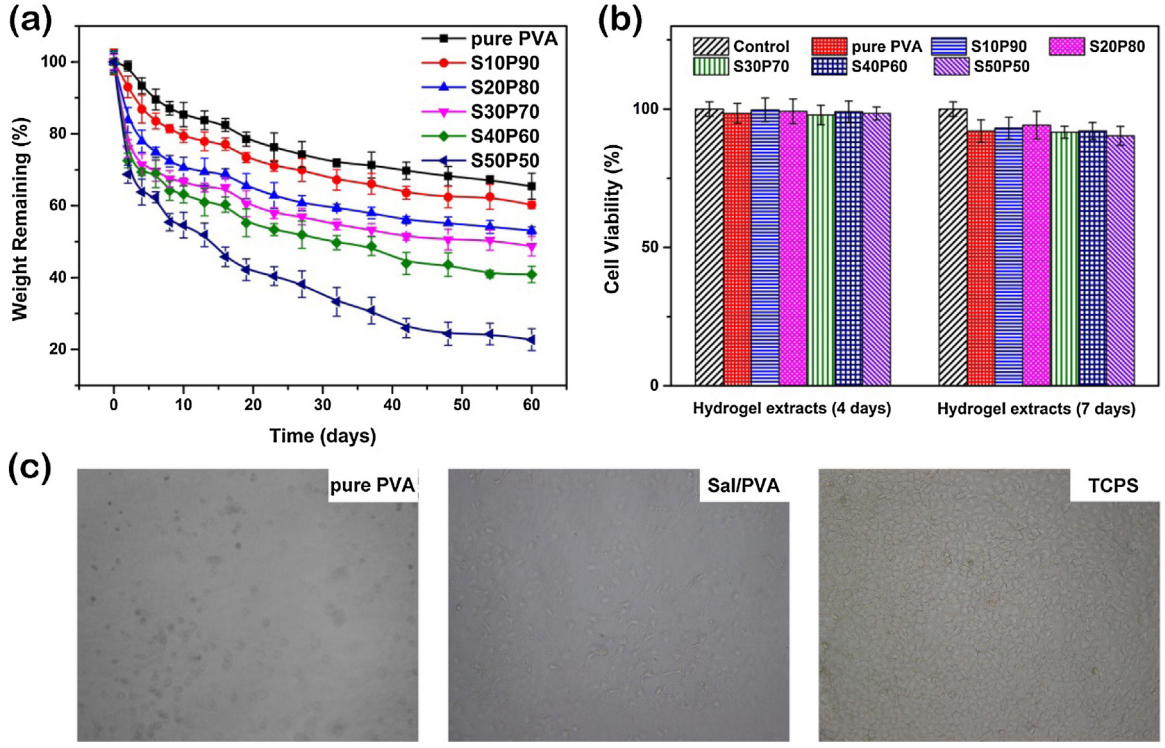

Fig. 6. Degradation (a) and cytotoxicity profile (b) of pure PVA and Sal/PVA hydrogels. (c) Optical microscope images (100×) of COS-7 cells cultured on the surface of TCPS, pure PVA and Sal/PVA hydrogels.

The reason for this consequence was mainly due to the cleavage of entanglement polymer chains (Hassan et al., 2000). Compared to the unfilled Salecan hydrogels, the pure PVA hydrogel with higher physical cross-linking density, which can restrained the disintegration of network, experienced surface erosion and degraded at a slower rate. These results suggested that the degradation rate of Sal/PVA gels can be manipulated by tailoring the composition ratio of Sal/PVA, which contributed to meet specific tissue-engineering requirements.

3.11. In vitro cell studies

3.11.1. Cytotoxicity of hydrogel extract

Fig. 6(b) shows the viability of COS-7 cells after an incubation period of 4 and 7 days. As seen in Fig. 6(b), the cell viability of all the samples was higher than 90% (compared with negative control group), indicating that Sal/PVA hydrogels were nontoxic to COS-7 cells. The excellent cell viability of the composite hydrogels was attributed to the good biocompatibility of the Salecan and the PVA, as well as a green fabrication process of the hydrogels.

3.11.2. Cell adhesion

The adhesion of COS-7 cells on the composite hydrogels was investigated by culturing the cells on thin hydrogel films (approximately 2 mm thickness). TCPS and pure PVA hydrogel served as positive and negative controls, respectively. After incubating for 5 days, cells did not spread on pure PVA hydrogel, as shown by their rounded shape (Fig. 6(c)). In contrast, cells cultured on Sal/PVA blending hydrogel films displayed spindle morphology similar to that observed on TCPS control, indicating favorable adhesion and spreading. These results clearly suggested that Sal/PVA hydrogels had better surface for the culture of COS-7 cells, which was related to the presence of Salecan in the pure PVA hydrogel. Analogous effects were noted by Liu et al. (2009), who demonstrated that the addition of nature polymers (starch, chitosan, collagen) to PVA stimulated cell adhesion.

Cell adhesion on 2D substrates is often dictated and controlled by the ability of proteins (either resident in serum or secreted by cells) to adsorb onto the material surface (Carbonetto, Gruver, & Turner, 1982; Nuttelman, Mortisen, Henry, & Anseth, 2001). Thus, an alternative possible explanation for the better adhesion and spreading of cells on the Sal/PVA membrane was that mediating proteins were richly adsorbed, retained, and the adhesion proteins took a configuration beneficial for cell spreading. In contrast, pure PVA hydrogels were non-cell adhesive (Alves, Jensen, Smith, & Zelikin, 2011; Chuang, Young, Yao, & Chiu, 1999). This may be due to that protein-binding sits on the PVA were not present or adsorbed proteins were distorted by the pure PVA surface (Chuang et al., 1999). In addition, compared with pure PVA hydrogel, Sal/PVA blending hydrogels possessed interconnecting porous structure due to the incorporation of Salecan (Hu et al., 2014b). Such porous network might allow effective nutrient supply, oxygen diffusion and metabolic waste removal, which was necessary for cell adhesion (Gnanaprakasam Thankam & Muthu, 2014).

4. Conclusion

In this paper, a novel Sal/PVA composite hydrogels were synthesized by a freeze/thaw method. The obtained cryogels are freedom from potential toxic species like bi-functional cross-linkers or initiators. The characteristics of Sal/PVA hydrogels were subjected to detailed analysis by FTIR, XRD, DSC, TGA and SEM. The SEM investigations showed that the morphology of the cryogels can be tailored by the Salecan content. In comparison to the pure PVA hydrogel, hybrid hydrogels exhibited a porous structure with internal diameter ranging from 2.8 to 13.2 μm. Results from XRD and DSC revealed that crystalline regions of the cryogels were depended on the content of the Salecan. With the increase of the Sal/PVA ratio, the percent crystallinity of the samples decreased dramatically. This may be indicative of improved interaction between the Salecan and PVA. FTIR spectra further confirmed the presence of the interactions, such as hydrogen bonds, between the two polymers of the cryogels. Rheological measurements indicated that storage modulus G' of the material can be enhanced by increasing the PVA content. The swelling capacities of the hybrid cryogels were elevated by the addition of Salecan in the network. In vitro degradation study demonstrated that introduction of certain amount Salecan into PVA hydrogels significantly accelerated the degradation rate. Indirect cytotoxicity assessment of the hydrogel revealed that the hydrogel was non-toxic to COS-7 cells. Furthermore, these hybrid Sal/PVA hydrogels can support cell adhesion. Compared to pure PVA hydrogels, the cell adhesion improved markedly when Salecan was incorporated into the PVA. Due to high water absorption ability, controllable modulus, tunable biodegradation and prominent biocompatibility, the Sal/PVA hybrid cryogels may be a promising material for biomedical applications especially in cell adhesion and tissue engineering.

Acknowledgments

This work was supported by National Natural Science Foundation of China under the Grant 30870625 and the Fundamental Research Funds for the Central Universities, NUST2011XQTR07.

Appendix A. Supplementary data

Supplementary data associated with this article can be found, in the online version, at http://dx.doi.org/10.1016/j.carbpol.2014.11.021.

References

Almany, L., & Seliktar, D. (2005). Biosynthetic hydrogel scaffolds made from fibrinogen and polyethylene glycol for 3D cell cultures. *Biomaterials*, *26*(15), 2467–2477.

Alves, M. H., Jensen, B. E., Smith, A. A., & Zelikin, A. N. (2011). Poly(vinyl alcohol) physical hydrogels: New vista on a long serving biomaterial. *Macromolecular Bioscience*, *11*(10), 1293–1313.

Aouada, F. A., Moura, M. R. d., Lopes da Silva, W. T., Muniz, E. C., & Mattoso, L. H. C. (2011). Preparation and characterization of hydrophilic, spectroscopic, and kinetic properties of hydrogels based on polyacrylamide and methylcellulose polysaccharide. *Journal of Applied Polymer Science*, *120*(5), 3004–3013.

Aouada, F. A., Pan, Z., Orts, W. J., & Mattoso, L. H. C. (2009). Removal of paraquat pesticide from aqueous solutions using a novel adsorbent material based on polyacrylamide and methylcellulose hydrogels. *Journal of Applied Polymer Science*, *114*(4), 2139–2148.

Autissier, A., Le Visage, C., Pouzet, C., Chaubet, F., & Letourneur, D. (2010). Fabrication of porous polysaccharide-based scaffolds using a combined freeze-drying/cross-linking process. *Acta Biomaterialia*, *6*(9), 3640–3648.

Bai, H., Li, C., Wang, X., & Shi, G. (2010). A pH-sensitive graphene oxide composite hydrogel. *Chemical Communications (Cambridge, England)*, *46*(14), 2376–2378.

Balakrishnan, B., Mohanty, M., Umashankar, P. R., & Jayakrishnan, A. (2005). Evaluation of an in situ forming hydrogel wound dressing based on oxidized alginate and gelatin. *Biomaterials*, *26*(32), 6335–6342.

Bortolin, A., Aouada, F. A., de Moura, M. R., Ribeiro, C., Longo, E., & Mattoso, L. H. C. (2012). Application of polysaccharide hydrogels in adsorption and controlled-extended release of fertilizers processes. *Journal of Applied Polymer Science*, *123*(4), 2291–2298.

Carbonetto, S., Gruver, M., & Turner, D. (1982). Nerve fiber growth on defined hydrogel substrates. *Science*, *216*(4548), 897–899.

Cascone, M. G., Maltinti, S., Barbani, N., & Laus, M. (1999). Effect of chitosan and dextran on the properties of poly(vinyl alcohol) hydrogels. *Journal of Materials Science: Materials in Medicine*, *10*(7), 431–435.

Chen, P., Wang, Z., Zeng, L., Wang, S., Dong, W., Jia, A., Cai, C., & Zhang, J. (2012). Protective effects of Salecan against carbon tetrachloride-induced acute liver injury in mice. *Journal of Applied Toxicology*, *32*(10), 796–803.

Chen, P., Wang, Z., Zeng, L., Yang, X., Wang, S., Dong, W., et al. (2011). A novel soluble beta-glucan Salecan protects against acute alcohol-induced hepatotoxicity in mice. *Bioscience, Biotechnology, and Biochemistry*, *75*(10), 1990–1993.

Chuang, W.-Y., Young, T.-H., Yao, C.-H., & Chiu, W.-Y. (1999). Properties of the poly(vinyl alcohol)/chitosan blend and its effect on the culture of fibroblast in vitro. *Biomaterials*, *20*(16), 1479–1487.

Costa-Júnior, E. S., Barbosa-Stancioli, E. F., Mansur, A. A. P., Vasconcelos, W. L., & Mansur, H. S. (2009). Preparation and characterization of chitosan/poly(vinyl alcohol) chemically crosslinked blends for biomedical applications. *Carbohydrate Polymers*, *76*(3), 472–481.

Dinu, M. V., Přádný, M., Drăgan, E. S., & Michálek, J. (2013a). Morphogical and swelling properties of porous hydrogels based on poly(hydroxyethyl methacrylate) and chitosan modulated by ice-templating process and porogen leaching. *Journal of Polymer Research*, *20*(11)

Dinu, M. V., Přádný, M., Drăgan, E. S., & Michálek, J. (2013b). Ice-templated hydrogels based on chitosan with tailored porous morphology. *Carbohydrate Polymers*, *94*(1), 170–178.

Dragan, E. S. (2014). Design and applications of interpenetrating polymer network hydrogels. A review. *Chemical Engineering Journal*, *243*, 572–590.

Dragan, E. S., & Apopei, D. F. (2013). Multiresponsive macroporous semi-IPN composite hydrogels based on native or anionically modified potato starch. *Carbohydrate Polymers*, *92*(1), 23–32.

El-Sherbiny, I. M. (2010). Enhanced pH-responsive carrier system based on alginate and chemically modified carboxymethyl chitosan for oral delivery of protein drugs: Preparation and in-vitro assessment. *Carbohydrate Polymers*, *80*(4), 1125–1136.

El-Sherbiny, I. M., Abdel-Hamid, M. I., Rashad, M., Ali, A. S. M., & Azab, Y. A. (2013). New calcareous soil–alginate composites for efficient uptake of Fe(III), Mn(II) and As(V) from water. *Carbohydrate Polymers*, *96*(2), 450–459.

El-Sherbiny, I. M., & Yacoub, M. H. (2013). Hydrogel scaffolds for tissue engineering: Progress and challenges. *Global Cardiology Science & Practice*, *2013*(3), 316–342.

Fathi, E., Atyabi, N., Imani, M., & Alinejad, Z. (2011). Physically crosslinked polyvinyl alcohol–dextran blend xerogels: Morphology and thermal behavior. *Carbohydrate Polymers*, *84*(1), 145–152.

Gnanaprakasam Thankam, F., & Muthu, J. (2014). Alginate based hybrid copolymer hydrogels—Influence of pore morphology on cell–material interaction. *Carbohydrate Polymers*, *112*, 235–244.

Gnanaprakasam Thankam, F., Muthu, J., Sankar, V., & Kozhiparambil Gopal, R. (2013). Growth and survival of cells in biosynthetic poly vinyl alcohol-alginate IPN hydrogels for cardiac applications. *Colloids and Surfaces B: Biointerfaces*, *107*, 137–145.

Hassan, C. M., & Peppas, N. A. (2000a). Structure and applications of poly(vinyl alcohol) hydrogels produced by conventional crosslinking or by freezing/thawing methods. *Biopolymers. PVA Hydrogels Anionic Polymerisation Nanocomposites*, *153*, 37–65.

Hassan, C. M., & Peppas, N. A. (2000b). Structure and morphology of freeze/thawed PVA hydrogels. *Macromolecules*, *33*(7), 2472–2479.

Hassan, C. M., Ward, J. H., & Peppas, N. A. (2000). Modeling of crystal dissolution of poly(vinyl alcohol) gels produced by freezing/thawing processes. *Polymer*, *41*(18), 6729–6739.

Hernández, R., Sarafian, A., López, D., & Mijangos, C. (2004). Viscoelastic properties of poly(vinyl alcohol) hydrogels and ferrogels obtained through freezing–thawing cycles. *Polymer*, *45*(16), 5543–5549.

Holloway, J. L., Spiller, K. L., Lowman, A. M., & Palmese, G. R. (2011). Analysis of the in vitro swelling behavior of poly(vinyl alcohol) hydrogels in osmotic pressure solution for soft tissue replacement. *Acta Biomaterialia*, *7*(6), 2477–2482.

Hu, X., Feng, L., Wei, W., Xie, A., Wang, S., Zhang, J., et al. (2014). Synthesis and characterization of a novel semi-IPN hydrogel based on Salecan and poly(*N*,*N*-dimethylacrylamide-*co*-2-hydroxyethyl methacrylate). *Carbohydrate Polymers*, *105*, 135–144.

Hu, X., Feng, L., Xie, A., Wei, W., Wang, S., Zhang, J., et al. (2014). Synthesis and characterization of a novel hydrogel: Salecan/polyacrylamide semi-IPN hydrogel with a desirable pore structure. *Journal of Materials Chemistry B*, *2*(23), 3646.

Huang, M., Cai, D., Liu, Y., Sun, J., Wang, J., Qin, C., et al. (2012). Investigation of a-PVA/s-PVA hydrogels prepared by freezing–thawing method. *Fibers and Polymers*, *13*(8), 955–962.

Huang, M. H., & Yang, M. C. (2008). Evaluation of glucan/poly(vinyl alcohol) blend wound dressing using rat models. *International Journal of Pharmaceutics*, *346*(1–2), 38–46.

Kaity, S., Isaac, J., & Ghosh, A. (2013). Interpenetrating polymer network of locust bean gum-poly(vinyl alcohol) for controlled release drug delivery. *Carbohydrate Polymers*, *94*(1), 456–467.

Kim, J. O., Park, J. K., Kim, J. H., Jin, S. G., Yong, C. S., Li, D. X., et al. (2008). Development of polyvinyl alcohol-sodium alginate gel-matrix-based wound dressing system containing nitrofurazone. *International Journal of Pharmaceutics*, *359*(1–2), 79–86.

Kobayashi, M., & Oka, M. (2004). Characterization of a polyvinyl alcohol-hydrogel artificial articular cartilage prepared by injection molding. *Journal of Biomaterials Science Polymer Edition*, *15*(6), 741–751.

Lin, W. C., Yu, D. G., & Yang, M. C. (2006). Blood compatibility of novel poly(gamma-glutamic acid)/polyvinyl alcohol hydrogels. *Colloids and Surfaces B: Biointerfaces*, *47*(1), 43–49.

Liu, Y., Vrana, N. E., Cahill, P. A., & McGuinness, G. B. (2009). Physically crosslinked composite hydrogels of PVA with natural macromolecules: structure, mechanical properties, and endothelial cell compatibility. *Journal of Biomedical Materials Research B: Applied Biomaterials*, *90*(2), 492–502.

Lozinsky, V. I., & Plieva, F. M. (1998). Poly(vinyl alcohol) cryogels employed as matrices for cell immobilization. 3. Overview of recent research and developments. *Enzyme and Microbial Technology*, *23*(3–4), 227–242.

Mansur, H. S., Costa, E. de S., Mansur, A. A. P., & Barbosa-Stancioli, E. F. (2009). Cytocompatibility evaluation in cell-culture systems of chemically crosslinked chitosan/PVA hydrogels. *Materials Science and Engineering: C*, *29*(5), 1574–1583.

Meng, X., Matson, J., & Edgar, K. J. (2014). Olefin cross-metathesis, a mild, modular approach to functionalized cellulose esters. *Polymer Chemistry*, http://dx.doi.org/10.1039/C4PY01102 C

Nishio, Y., & Manley, R. S. J. (1988). Cellulose-poly(vinyl alcohol) blends prepared from solutions in *N*,*N*-dimethylacetamide-lithium chloride. *Macromolecules*, *21*(5), 1270–1277.

Nuttelman, C. R., Mortisen, D. J., Henry, S. M., & Anseth, K. S. (2001). Attachment of fibronectin to poly(vinyl alcohol) hydrogels promotes NIH3T3 cell adhesion, proliferation, and migration. *Journal of Biomedical Materials Research*, *57*(2), 217–223.

Ossipov, D., Kootala, S., Yi, Z., Yang, X., & Hilborn, J. (2013). Orthogonal chemoselective assembly of hyaluronic acid networks and nanogels for drug delivery. *Macromolecules*, *46*(10), 4105–4113.

Peppas, N. A., & Hansen, P. J. (1982). Crystallization kinetics of poly(vinyl alcohol). *Journal of Applied Polymer Science*, *27*(12), 4787–4797.

Peppas, N. A., & Stauffer, S. R. (1991). Reinforced uncrosslinked poly(vinyl alcohol) gels produced by cyclic freezing–thawing processes: A short review. *Journal of Controlled Release*, *16*(3), 305–310.

Plieva, F. M., Karlsson, M., Aguilar, M.-R., Gomez, D., Mikhalovsky, S., Galaev, I. Y., et al. (2006). Pore structure of macroporous monolithic cryogels prepared from poly(vinyl alcohol). *Journal of Applied Polymer Science*, *100*(2), 1057–1066.

Sahoo, S. K., Panyam, J., Prabha, S., & Labhasetwar, V. (2002). Residual polyvinyl alcohol associated with poly(D,L-lactide-*co*-glycolide) nanoparticles affects their physical properties and cellular uptake. *Journal of Controlled Release*, *82*(1), 105–114.

Slaughter, B. V., Khurshid, S. S., Fisher, O. Z., Khademhosseini, A., & Peppas, N. A. (2009). Hydrogels in regenerative medicine. *Advanced Materials*, *21*(32–33), 3307–3329.

Sung, J. H., Hwang, M. R., Kim, J. O., Lee, J. H., Kim, Y. I., Kim, J. H., et al. (2010). Gel characterisation and in vivo evaluation of minocycline-loaded wound dressing with enhanced wound healing using polyvinyl alcohol and chitosan. *International Journal of Pharmaceutics*, *392*(1–2), 232–240.

Wu, J., Gong, X., Fan, Y., & Xia, H. (2011). Physically crosslinked poly(vinyl alcohol) hydrogels with magnetic field controlled modulus. *Soft Matter*, *7*(13), 6205.

Xiu, A., Kong, Y., Zhou, M., Zhu, B., Wang, S., & Zhang, J. (2010). The chemical and digestive properties of a soluble glucan from *Agrobacterium* sp. ZX09. *Carbohydrate Polymers*, *82*(3), 623–628.

Xiu, A., Zhan, Y., Zhou, M., Zhu, B., Wang, S., Jia, A., et al. (2011). Results of a 90-day safety assessment study in mice fed a glucan produced by *Agrobacterium* sp. ZX09. *Food and Chemical Toxicology*, *49*(9), 2377–2384.

Xiu, A., Zhou, M., Zhu, B., Wang, S., & Zhang, J. (2011). Rheological properties of Salecan as a new source of thickening agent. *Food Hydrocolloids*, *25*(7), 1719–1725.

Yang, C., Xu, L., Zhou, Y., Zhang, X., Huang, X., Wang, M., et al. (2010). A green fabrication approach of gelatin/CM-chitosan hybrid hydrogel for wound healing. *Carbohydrate Polymers*, *82*(4), 1297–1305.

Yang, D., Yu, K., Ai, Y., Zhen, H., Nie, J., & Kennedy, J. F. (2011). The mineralization of electrospun chitosan/poly(vinyl alcohol) nanofibrous membranes. *Carbohydrate Polymers*, *84*(3), 990–996.

Zhang, R., & Edgar, K. J. (2014). Synthesis of curdlan derivatives regioselectively modified at C-6: O-(*N*)-acylated 6-amino-6-deoxycurdlan. *Carbohydrate Polymers*, *105*, 161–168.